OH-Cu-OH planes is 16.5 and 6.1° for hexafluorophosphate and sulfate complexes, respectively, and in both cases the observed J values are lower than predicted from the linear relationship. In the centrosymmetric nitrate, perchlorate, and squarate complexes, no bending is present. Evidence of attenuation in the antiferromagnetic coupling has been found in two hydroxo-bridged dinuclear compounds with OCuO/OCuO dihedral angles of 147.5 and 132.9°, respectively.[30-32]

We would finish this structural discussion with a brief comment on the key role of the counterion in such a series of complexes. In all these complexes the counterion is semicoordinated: the perchlorate and sulfate complexes are built of isolated $[(bpy)Cu(OH)_2Cu(bpy)]^{2+}$ units containing bismonodentate perchlorate and monodentate sulfate respectively; for the nitrate and squarate complexes, a one-dimensional arrangement of $[(bpy)Cu(OH)_2Cu(bpy)]^{2+}$ is observed, the squarate acting in a 1,3-bismonodentate fashion and the nitrate linking a copper atom of a dinuclear unit with a hydroxo group of another unit through two of its oxygen atoms. Finally, when hexafluorophosphate is used as a counterion, the tetranuclear entity herein described is obtained. To summarize, this series provides an example of the relevant structural role of the counterion and consequently of its influence on the magnetic properties of the resulting compounds.

Acknowledgment. We thank the Comisiôn Interministerial de Ciencia y Technologîa (Spain) (Project PB88-0490) and the Programme d'Actions Integrées Franco-Espagnoles for partial financial support. We are also indebted to Professor O. Kahn for his continuous interest in this work.

Supplementary Material Available: Crystallographic data (Table SI), anisotropic thermal parameters (Table SII), hydrogen coordinates (Table SIII), bond distances and angles within the PF_6^- ions (Table SV), bond angles in the cluster (Table SVI), and a crystal packing diagram (Figure S1) (8 pages); observed and calculated structure factors (Table SIV) (17 pages). Ordering information is given on any current masthead page. A listing of experimental magnetic data is available from the authors on request.

(30) Charlot, M. F.; Kahn, O.; Jeannin, S.; Jeannin, Y. *Inorg. Chem.* **1980**, *19*, 1410.
(31) Charlot, M. F.; Jeannin, S.; Jeannin, Y.; Kahn, Lucrece-Abaul, J.; Martin-Frere, J. *Inorg. Chem.* **1979**, *18*, 1675.
(32) Iitaka, Y.; Shimizu, K.; Kwan, T. *Acta Crystallogr.* **1966**, *20*, 803.

Contribution No. 8130 from the Arnold and Mabel Beckman Laboratories of Chemical Synthesis, California Institute of Technology, Pasadena, California 91125

Synthesis and Structural Characterization of Binuclear Ruthenium Aquo, Hydroxy, and Oxo Complexes Incorporating the Anionic Tripod Ligand $[(\eta^5\text{-}C_5H_5)Co\{(CH_3CH_2O)_2P{=}O\}_3]^-$

John M. Power, Kaspar Evertz, Larry Henling, Richard Marsh, William P. Schaefer, Jay A. Labinger,* and John E. Bercaw*

Received June 6, 1990

The two-phase reaction of NaL_{OEt} (L_{OEt}^- = $[CpCo\{(EtO)_2P{=}O\}_3]^-$) in 1% H_2SO_4 with RuO_4 in CCl_4 generates the Ru^{IV}-Ru^{IV} edge-sharing bioctahedral complex $[L_{OEt}(H_2O)Ru(\mu\text{-}O)_2Ru(OH_2)L_{OEt}][SO_4]$, in the aqueous phase. This bis(aquo) dication can be isolated as the PF_6^- salt or, alternatively, treated with excess Na_2CO_3 to produce the neutral bis(hydroxo) species $[L_{OEt}(HO)Ru(\mu\text{-}O)_2Ru(OH)L_{OEt}]$ in 50% yield, which in turn can be treated with CF_3SO_3H to regenerate the bis(aquo) complex $[L_{OEt}(H_2O)Ru(\mu\text{-}O)_2Ru(OH_2)L_{OEt}][CF_3SO_3]_2$ quantitatively. The reaction of $[L_{OEt}(HO)Ru(\mu\text{-}O)_2Ru(OH)L_{OEt}]$ with RuO_4 in CCl_4 produces the Ru^V-Ru^V-dioxo species $[L_{OEt}(O)Ru(\mu\text{-}O)_2Ru(O)L_{OEt}]$ in 65% yield. $[L_{OEt}(H_2O)Ru(\mu\text{-}O)_2Ru(OH_2)L_{OEt}][CF_3SO_3]_2$, $[L_{OEt}(HO)Ru(\mu\text{-}O)_2Ru(OH)L_{OEt}]$, and $[L_{OEt}(O)Ru(\mu\text{-}O)_2Ru(O)L_{OEt}]$ have been characterized by X-ray crystallography. The Ru^{IV}-Ru^{IV} species exhibit a substantial metal-metal interaction (Ru-Ru is 2.452 Å in $[L_{OEt}(HO)Ru(\mu\text{-}O)_2Ru(OH)L_{OEt}]$ and 2.505 Å in $[L_{OEt}(H_2O)Ru(\mu\text{-}O)_2Ru(OH_2)L_{OEt}][CF_3SO_3]_2$), while the Ru^V-Ru^V complex, although diamagnetic, shows a relatively weak interaction (2.912 Å). Crystal data: $[L_{OEt}(H_2O)Ru(\mu\text{-}O)_2Ru(OH_2)L_{OEt}][CF_3SO_3]_2$, $Ru_2Co_2C_{36}H_{74}O_{28}P_6S_2F_6$, triclinic, $P\bar{1}$, with a = 10.510 (6) Å, b = 13.475 (6) Å, c = 14.132 (9) Å, α = 101.50 (5)°, β = 117.99 (5)°, γ = 101.42 (5)°, V = 1630.6 (16) Å^3, Z = 1, $R(F_o)$ = 0.0483; $[L_{OEt}(HO)Ru(\mu\text{-}O)_2Ru(OH)L_{OEt}]\cdot 4C_6H_5CH_3$, $Ru_2Co_2C_{62}H_{104}O_{22}P_6$, monoclinic, $P2_1/n$, with a = 13.187 (5) Å, b = 23.103 (8) Å, c = 13.455 (6) Å, β = 113.82 (4)°, V = 3750 (3) Å^3, Z = 2, $R(F_o)$ = 0.0563; $[L_{OEt}(O)Ru(\mu\text{-}O)_2Ru(O)L_{OEt}]$, $Ru_2Co_2C_{34}H_{70}O_{22}P_6$, monoclinic, $C2/c$, with a = 27.486 (7) Å, b = 11.849 (5) Å, c = 17.268 (7) Å, β = 109.11 (3)°, V = 5314 (5) Å^3, Z = 4, $R(F_o)$ = 0.0610.

Introduction

Interest in high-valent ruthenium oxo complexes has stemmed in part from the realization that the ruthenyl (Ru=O) center can be stabilized by judicious choice of ancillary ligand without greatly decreasing its oxidizing power. In this context, the successful use of oxidatively robust nitrogen-based ligands such as porphyrins, polypyridyls, and macrocyclic tertiary amines has led to a range of structurally characterized high-valent ($Ru^{IV} \rightarrow Ru^{VI}$) oxo derivatives.[1] In virtually all of these systems the ancillary ligands preferentially occupy the equatorial sites of an octahedral ruthenium center. While the oxidizing potential of these ruthenium complexes is found to vary somewhat with the electronic nature of the ligand, a more profound effect might be brought about by changing the coordination requirements of the ancillary ligand. Indeed, Meyer and others have noted that *cis*-dioxoruthenium(VI) complexes should be more powerful oxidants than their trans counterparts.[2] Apart from two recent reports of such complexes that utilize bulky polypyridyls to confer a cis configuration on the oxo ligands,[2c,d] very little effort has been directed at the search for alternate ligand systems[3]—not only for this specific case but

(1) For example: Groves, J. T.; Quinn, R. *Inorg. Chem.* **1984**, *23*, 3844. Groves, J. T.; Ahn, K.-H. *Inorg. Chem.* **1987**, *26*, 3831. Moyer, B. A.; Meyer, T. J. *Inorg. Chem.* **1981**, *20*, 436. Takeuchi, K. J.; Thompson, M. S.; Pipes, D. W.; Meyer, T. J. *Inorg. Chem.* **1984**, *23*, 1845. Dobson, J. C.; Meyer, T. J. *Inorg. Chem.* **1988**, *27*, 3283. Che, C.-M.; Lai, T.-F.; Wong, K.-Y. *Inorg. Chem.* **1987**, *26*, 2289. Che, C.-M.; Tang, W.-T.; Lee, W.-O.; Wong, W.-T.; Lai, T.-F. *J. Chem. Soc., Dalton Trans.* **1989**, 2011. Che, C.-M.; Tang, W.-T.; Wong, W.-T.; Lai, T.-F. *J. Am. Chem. Soc.* **1989**, *111*, 9048.

(2) (a) Takeuchi, K. J.; Samuels, G. J.; Gersten, S. W.; Gilbert, J. A.; Meyer, T. J. *Inorg. Chem.* **1983**, *22*, 1409. (b) Collin, J. P.; Sauvage, J. P. *Inorg. Chem.* **1986**, *25*, 135. (c) Bailey, C. L.; Drago, R. S. *J. Chem. Soc., Chem. Commun.* **1987**, 179. (d) Che, C.-M.; Leung, W.-H. *J. Chem. Soc., Chem. Commun.* **1987**, 1376.

(3) Alternate N-based ligands: (a) Llobet, A.; Doppelt, P.; Meyer, T. J. *Inorg. Chem.* **1988**, *27*, 514. (b) Che, C.-M.; Yam, V. W.-W.; Mak, T. C. W. *J. Am. Chem. Soc.* **1990**, *112*, 2284.

0020-1669/90/1329-5058$02.50/0

for broader application to high-oxidation-state transition-metal complexes in general. Clearly, one approach would be to utilize an ancillary ligand that could only coordinate facially to the ruthenium center.

The anionic cobalt(III)-based oxygen tripod ligand (L_{OEt}^-) developed by Kläui and coworkers[4a-f] seems to be an ideal system for this purpose. It is in many ways similar to the cyclopentadienyl

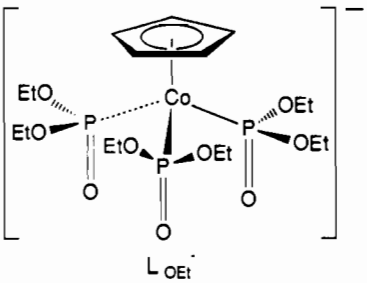

(Cp) ligand and its derivatives, which have been the workhorses of organometallic chemistry. However, it is likely that this trischelating ligand may be considerably more oxidatively robust than the Cp ligand and hence better suited for use in ruthenium oxo chemistry. Indeed, L_{OEt}^- has been shown to complex Ce^{IV},[4d] suggesting that it should be stable under strongly oxidizing conditions. Furthermore, its characterization as a hard, weak-ligand-field ligand, similar to hydroxide and fluoride ions,[4c] should also make it compatible with high-oxidation-state ruthenium centers. Interestingly, because L_{OEt}^- binds exclusively through oxygen, it has recently been employed in modeling studies of the iron-containing enzymes methane monooxygenase and ribonucleotide reductase, which have been shown by EXAFS to contain a high degree of oxygen coordination at the iron centers.[4g]

Herein we report that our initial endeavors at synthesizing high-oxidation-state ruthenium derivatives with the L_{OEt}^- ligand have led to a set of binuclear aquo, hydroxy, and oxo complexes, which have been spectroscopically and structurally characterized.

Experimental Section

General Considerations. CpLi, $(EtO)_2P(O)H$, NaCN, KPF_6, CF_3SO_3H (Aldrich), $Co(acac)_2$ (Alfa), $RuCl_3 \cdot xH_2O$ (Aesar) were used as supplied. All other solvents and chemicals were of analytical grade and were used without further purification. $L_{OEt}Na$ and RuO_4 were synthesized by published procedures.[4a,5]

Elemental analyses were performed at the Caltech Analytical Laboratory by Fenton Harvey and at Oneida Research Services, Inc., Whitesboro, NY. Infrared spectra were recorded either as Nujol mulls on KBr plates or as KBr pellets on a Perkin-Elmer Model 1600 FT-IR spectrophotometer. ^1H NMR spectra were recorded on a JEOL GX400Q (399.78 MHz) instrument in either CD_2Cl_2 (5.32) or C_6D_6 (7.15) solutions. $^{31}P\{^1H\}$ spectra were recorded on a JEOL FX-90Q instrument (36.3 MHz; vs H_3PO_4). UV–vis spectra were recorded on a Cary 14 UV–vis spectrophotometer in acetonitrile solutions.

$[L_{OEt}(H_2O)Ru(\mu\text{-}O_2)Ru(OH_2)L_{OEt}][PF_6]_2$. A CCl_4 solution of RuO_4 (22 mL of a 13 g L^{-1} solution, 1.8 mmol) was added dropwise to a solution of $L_{OEt}Na$ (1.2 g, 2.2 mmol) in 1% H_2SO_4 (20 mL, 2.2 mmol) at 0 °C. During the addition the color of the mixture changed from clear yellow to dark red-brown. This mixture was stirred at 0 °C for 30 min and for a further 90 min at 25 °C. The dark green aqueous layer was separated from the organic layer and cooled to 0 °C. A solution of KPF_6 (0.78 g, 4.2 mmol) in a minimal amount of H_2O (ca. 2 mL) was added to the cooled aqueous layer. An olive green precipitate formed immediately. After 15 min at 0 °C the product was isolated on a medium frit and washed with distilled H_2O (2 × 10 mL) (0.67 g, 48%). Anal. Calcd for $C_{34}H_{74}Co_2F_{12}O_{22}P_8Ru_2$ (mol wt 1630.80): C, 25.04; H, 4.57. Found: C, 24.51; H, 4.40. IR (Nujol): ν_{max} 3460 (br, s), 3125 (w), 1300 (w), 1165 (m), 1105 (s), 1064 (vs), 1023 (br, vs), 956 (s), 944 (s), 846 (vs), 835 (sh), 777 (m), 741 (m), 619 (m), 602 (sh), 558 (m), 500 (w), 456 (w) cm^{-1}. ^1H NMR (CD_2Cl_2): δ 5.25 (br s, H_2O, 2 H), 5.17 (s, C_5H_5, 5 H), 4.49 (m, OCH_2CH_3, 4 H), 4.23 (m, OCH_2CH_3, 2 H), 4.11 (m, OCH_2CH_3, 2 H), 3.82 (m, OCH_2CH_3, 4 H), 1.46 (t, J = 7.08 Hz, OCH_2CH_3, 6 H), 1.29 (t, J = 7.08 Hz, OCH_2CH_3, 6 H), 1.24 (t, J = 7.08 Hz, OCH_2CH_3, 6 H). $^{31}P\{^1H\}$ NMR (CD_2Cl_2): δ −144 (sept, J = 713 Hz, PF_6), +119 to +128 (m, $P(O)(OCH_2H_3)_2$). UV–vis (λ_{max}, nm (ϵ, M^{-1} cm^{-1}), in CH_3CN): 242 (58 000), 340 (14 200), 632 (2600).

$[L_{OEt}(HO)Ru(\mu\text{-}O)_2Ru(OH)L_{OEt}]$. The procedure for $[L_{OEt}(H_2O)Ru(\mu\text{-}O)_2Ru(OH_2)L_{OEt}][PF_6]_2$ (starting with 17 mmol of $L_{OEt}Na$) was followed as far as the isolation of the aqueous phase. After cooling of the green solution to 0 °C, an excess of an aqueous Na_2CO_3 solution was added slowly to control the evolution of CO_2. The resulting green precipitate was isolated on a medium frit and washed with distilled water (3 × 25 mL) (4.83 g, 52%). Anal. Calcd for $C_{34}H_{72}Co_2O_{22}P_6Ru_2$ (mol wt 1338.84): C, 30.50; H, 5.42. Found: C, 29.78; H, 5.11. IR (KBr): ν_{max} 3448 (br, s), 2978 (s), 2928 (m), 2903 (m), 2867 (sh, w), 1699 (sh, w), 1650 (br, m), 1478 (w), 1442 (m), 1425 (m), 1388 (s), 1364 (w), 1161 (sh, s), 1106 (br, vs), 1072 (br, vs), 1033 (br, vs), 938 (vs), 834 (s), 774 (s), 735 (s), 694 (sh, m), 668 (sh, w), 607 (br, vs), 496 (m) cm^{-1}. ^1H NMR (C_6D_6): δ 4.74 (s, C_5H_5, 5 H), 4.51 (m, OCH_2CH_3, 2 H), 4.36 (m, OCH_2CH_3, 6 H), 4.14 (m, OCH_2CH_3, 4 H), 1.23 (t, J = 7.08 Hz, OCH_2CH_3, 6 H), 1.21 (t, J = 7.08 Hz, OCH_2CH_3, 6 H), 1.09 (t, J = 6.96 Hz, OCH_2CH_3, 6 H). $^{31}P\{^1H\}$ NMR (C_6D_6): δ + 116 (vbr s, $P(O)(OCH_2H_3)_2$). UV–vis (λ_{max}, nm (ϵ, M^{-1} cm^{-1}), in CH_3CN): 242 (57 100), 340 (13 400), 694 (1900).

$[L_{OEt}(H_2O)Ru(\mu\text{-}O)_2Ru(OH_2)L_{OEt}][CF_3SO_3]_2$. A slight excess of CF_3SO_3H (0.1 mL) was added to a suspension of $[L_{OEt}(HO)Ru(\mu\text{-}O)_2Ru(OH)L_{OEt}]$ (0.5 g, 0.4 mmol) in H_2O (20 mL). The color of the solid changed almost immediately from a pale green to a bright (almost luminescent) green. (The formation of a solution was not observed.) The slurry was stirred for 15 min, after which the product was isolated on a medium frit and washed with distilled H_2O (0.6 g, 92%). Anal. Calcd for $C_{36}H_{74}Co_2F_6O_{28}P_6Ru_2S_2$ (mol wt 1638.93): C, 26.38; H, 4.55. Found: C, 26.34; H, 4.53. IR (KBr): ν_{max} 3126 (br, m), 2984 (s), 2932 (m), 2908 (m), 2870 (sh), 1479 (w), 1443 (w), 1428 (w), 1391 (m), 1299 (vs), 1239 (vs), 1222 (s), 1159 (vs), 1100 (s), 1062 (sh, vs), 1027 (br, vs), 950 (vs), 932 (sh, vs), 844 (m), 838 (sh, m), 815 (sh, w), 776 (s), 755 (m), 789 (m), 700 (w), 637 (vs), 613 (br, vs) cm^{-1}. ^1H NMR ($CDCl_3$): δ 6.56 (br s, H_2O, 2 H), 5.08 (s, C_5H_5, 5 H), 4.47 (m, OCH_2CH_3, 4 H), 4.23 (m, OCH_2CH_3, 2 H), 4.14 (m, OCH_2CH_3, 2 H), 3.81 (m, OCH_2CH_3, 4 H), 1.44 (t, J = 6.84 Hz, OCH_2CH_3, 6 H), 1.27 (t, J = 7.33 Hz, OCH_2CH_3, 6 H), 1.22 (t, J = 7.32 Hz, OCH_2CH_3, 6 H). $^{31}P\{^1H\}$ NMR (CD_2Cl_2): δ +117 to +134 (m, $P(O)(OCH_2H_3)_2$). UV–vis (λ_{max}, nm (ϵ, M^{-1} cm^{-1}), in CH_3CN): 242 (58 500), 339 (13 700), 635 (2000).

$[L_{OEt}(O)Ru(\mu\text{-}O)_2Ru(O)L_{OEt}]$. A CCl_4 solution of RuO_4 (11.1 mL of a 13 g L^{-1} solution, 0.87 mmol) was added dropwise to a slurry of $[L_{OEt}(HO)Ru(\mu\text{-}O)_2Ru(OH)L_{OEt}]$ (1.12 g, 0.83 mmol) also in CCl_4 (30 mL) at 20 °C. Almost immediately, the green color began to darken and by complete addition had become a deep purple. The solution was stirred for 3 h, filtered through Celite, and washed once with a 0.1 M solution of $NaHCO_3$. The solvent was removed in vacuo and the residue thoroughly dried over a period of 6 h. Recrystallization from CCl_4/*n*-pentane (1:5) at −60 °C gave the product as a purple microcrystalline solid (0.72 g, 65%). Anal. Calcd for $C_{34}H_{70}Co_2O_{22}P_6Ru_2$ (mol wt 1336.82): C, 30.55; H, 5.28. Found: C, 31.39; H, 5.33. IR (KBr): ν_{max} 2977 (s), 2924 (m), 2904 (m), 2867 (sh, w), 1640 (br, w), 1477 (w), 1443 (w), 1442 (w), 1387 (m), 1160 (sh, m), 1106 (br, vs), 1071 (br, vs), 1034 (br, vs), 934 (br, vs), 848 (s), 832 (s), 773 (s), 734 (m), 698 (sh, w), 609 (br, s), 497 (w) cm^{-1}. ^1H NMR (C_6D_6): δ 4.73 (s, C_5H_5, 5 H), 4.58 (m, OCH_2CH_3, 3 H), 4.47 (m, OCH_2CH_3, 3 H), 3.97 (m, OCH_2CH_3, 6 H), 1.38 (t, J = 7.08 Hz, OCH_2CH_3, 6 H), 1.02 (t, J = 7.08 Hz, OCH_2CH_3, 6 H), 0.97 (t, J = 7.08 Hz, OCH_2CH_3, 6 H). $^{31}P\{^1H\}$ NMR (C_6D_6): δ +115 to +118 (m, $P(O)(OCH_2H_3)_2$). UV–vis (λ_{max}, nm (ϵ, M^{-1} cm^{-1}), in CH_3CN): 242 (57 000), 333 (12 900), 557 (3900).

Structure of $[L_{OEt}(H_2O)Ru(\mu\text{-}O)_2Ru(OH_2)L_{OEt}][CF_3SO_3]_2$. Green single crystals of $[L_{OEt}(H_2O)Ru(\mu\text{-}O)_2Ru(OH_2)L_{OEt}][CF_3SO_3]_2$ were grown by slow diffusion of *n*-pentane into a chloroform solution at ambient temperature. A suitable crystal was selected, mounted in a capillary with silicon grease, and centered on a CAD-4 diffractometer using Mo Kα radiation. Unit cell parameters and an orientation matrix were obtained by a least-squares calculation from the setting angles of 24 reflections with 30° < 2θ < 43°. Two equivalent data sets were collected out to 2θ = 50°. The data were corrected for absorption and decay. Lorentz and polarization factors were applied, and two data sets were then merged (R = 0.020) to yield the final data set. Preliminary photographs and the diffractometer data showed the space group to be either $P1$ or $P\bar{1}$, with the latter yielding a satisfactory solution.

(4) (a) Kläui, W. *Z. Naturforsch., B.: Anorg. Chem., Org. Chem.* **1979**, *34B*, 1403. (b) Kläui, W. *Chem. Ber.* **1978**, *111*, 451. (c) Kläui, W.; Otto, H.; Eberspach, W.; Buchholz, E. *Chem. Ber.* **1982**, *115*, 1922. (d) Kläui, W.; Eberspach, W.; Schwarz, R. *J. Organomet. Chem.* **1983**, *252*, 347. (e) Kläui, W.; Müller, A.; Eberspach, W.; Boese, R.; Goldberg, I. *J. Am. Chem. Soc.* **1987**, *109*, 164. (f) For a review see: Kläui, W. *Angew. Chem., Int. Ed. Engl.* **1990**, *29*, 627. (g) Feng, X.; Bott, S. G.; Lippard, S. J. *J. Am. Chem. Soc.* **1989**, *111*, 8046.

(5) Griffith, W. P.; Pawson, D. *J. Chem. Soc., Dalton Trans.* **1973**, 1315.

A Patterson map gave the ruthenium atom coordinates. The remaining non-hydrogen atoms were located via successive structure factor–Fourier calculations. Five of the six terminal methyl groups were modeled with two positions, the total populations of each pair constrained to unity. The disorder in the anion was not interpreted. Hydrogen atom positions were determined from a difference map for the coordinated water and by calculation for the remainder. All hydrogen atoms were given isotropic B values 20% greater than that of the attached atom. No hydrogen parameters were refined. The disordered carbon atoms were refined with population and isotropic displacement parameters; all other non-hydrogen atoms were treated anisotropically. The complete least-squares matrix, consisting of non-hydrogen atomic parameters and a scale factor, contained 370 variables. A final difference Fourier map showed deviations ranging from −0.99 to +1.40 e Å^{-3}. However, all features greater than |0.5| e Å^{-3} can be attributed to disorder of the triflate anion. The refinement converged with an R factor of 0.0483 (0.0420 for $F_o^2 > 3\sigma(F_o^2)$) and a goodness of fit of 2.65 for all 5718 reflections.

Calculations were done on a VAX 11/750 computer with programs of the CRYM Crystallographic Computing System and ORTEP. Scattering factors and corrections for anomalous scattering were taken from a standard reference.[6a] $R = \sum||F_o| - |F_c||/\sum F_o$, for only $F_o^2 > 0$, and goodness of fit = $[\sum w(F_o^2 - F_c^2)^2/(n-p)]^{1/2}$, where n is the number of data and p the number of parameters refined. The function minimized in least squares was $\sum w(F_o^2 - F_c^2)^2$, where $w = 1/\sigma^2(F_o^2)$. Variances of the individual reflections were assigned on the basis of counting statistics plus an additional term, $0.014I^2$. Variances of the merged reflections were determined by standard propagation of error plus another additional term, $0.014I^2$. The absorption correction was done by Gaussin integration over an 8 × 8 × 8 grid. Transmission factors varied from 0.66 to 0.90.

Structure of $[L_{OEt}(HO)Ru(\mu\text{-}O)_2Ru(OH)L_{OEt}]$. Black-green trapezoids of **2** were grown by cooling of a concentrated toluene/petroleum ether (1:1) solution to −60 °C. Crystals of $[L_{OEt}(HO)Ru(\mu\text{-}O)_2Ru(OH)L_{OEt}]$ lose solvent rapidly, so they were coated with a layer of hydrocarbon oil upon removal from the flask. A suitable crystal was selected, attached to a glass fiber by silicon grease, and immediately placed in the low-temperature N_2 stream of a Syntex $P2_1$ diffractometer equipped with a modified LT-1 low-temperature device and using Mo Kα radiation with a graphite monochromator. Monoclinic lattice constants were determined by least-squares fit of 22 accurately centered reflections with 30° < 2θ < 48°. A data set was collected out to 2θ = 45° at 130 K by an ω-scan method. Absorption corrections were made by using the program XABS.[6b]

The structure was solved by the Patterson method. All non-hydrogen atoms, except those of the toluene solvate molecules, were refined with anisotropic thermal parameters. Hydrogen atoms were included by using a riding model with C–H = 0.96 Å and $U_{iso}(H) = 1.2U^*_{iso}(C)$, where U^*_{iso} is the equivalent isotropic thermal parameter. The complete least-squares matrix, consisting of non-hydrogen atomic parameters, contained 378 variables. A final difference Fourier map showed deviations ranging from 1.26 to 0.92 e Å^{-3} close to ruthenium. The refinement converged with an R factor of 0.0563.

The computer programs used were from SHELXTL, version 5, installed on a Data General Eclipse computer. $R = \sum||F_o| - |F_c||/|F_o|$. Neutral-atom scattering factors and corrections for anomalous dispersions were taken from the standard text.[6a]

Structure of $[L_{OEt}(O)Ru(\mu\text{-}O)_2Ru(O)L_{OEt}]$. Purple-brown single crystals of $[L_{OEt}(O)Ru(\mu\text{-}O)_2Ru(O)L_{OEt}]$ were grown by slow diffusion of n-pentane into a toluene solution at ambient temperature. A suitable crystal was selected, glued with epoxy to a glass fiber, and centered on a CAD-4 diffractometer; cell parameters and the orientation matrix were obtained from the setting angles of 25 reflections with 25° < 2θ < 30°. Two sets of data were collected to 2θ = 55°; after merging, Lorentz and polarization corrections were applied and the data were put on an approximately absolute scale by Wison's method. No absorption correction was applied ($\mu r_{max} = 0.39$).

The ruthenium atoms were located on a Patterson map, and subsequent structure factor–Fourier cycles led to the locations of the remaining atoms. Full-matrix least-squares refinement (303 parameters) gave the final model. Hydrogen atoms were introduced at an intermediate stage as fixed contributions to the structure factors at calculated positons (C–H = 0.95 Å) or, for methyl hydrogen atoms, at idealized positions based on difference maps calculated in their expected planes; they were repositioned once or twice, but never refined. The final matrix included coordinates and anisotropic thermal parameters for all non-hydrogen atoms and a scale factor. Hydrogen atoms were assigned isotropic thermal parameters, B, of 12.0 Å^2. The largest shift in the final cycle was 0.2σ in the y coordinate of atoms Cp2 and Cp3. The largest peaks in the final difference map were +0.57 and −0.62 e Å^{-3}; the peaks above |0.5 e Å^{-3}| were all but one (which was near ruthenium) near ethoxy groups and formed no interpretable pattern. The final R index for those 4070 reflections with $F_o^2 > 3\sigma(F_o^2)$ is 0.042. (See structure of $[L_{OEt}(H_2O)Ru(\mu\text{-}O)_2Ru(OH_2)L_{OE}3t][CF_3SO_3]_2$ for calculation procedures.)

The crystal, data collection, and refinement parameters for all three complexes are given in Table I. Tables II–IV contain the non-hydrogen coordinates and displacement parameters for $[L_{OEt}(H_2O)Ru(\mu\text{-}O)_2Ru(OH_2)L_{OEt}][CF_3SO_3]_2$, $[L_{OEt}(HO)Ru(\mu\text{-}O)_2Ru(OH)L_{OEt}]$, and $[L_{OEt}(O)Ru(\mu\text{-}O)_2Ru(O)L_{OEt}]$, respectively.

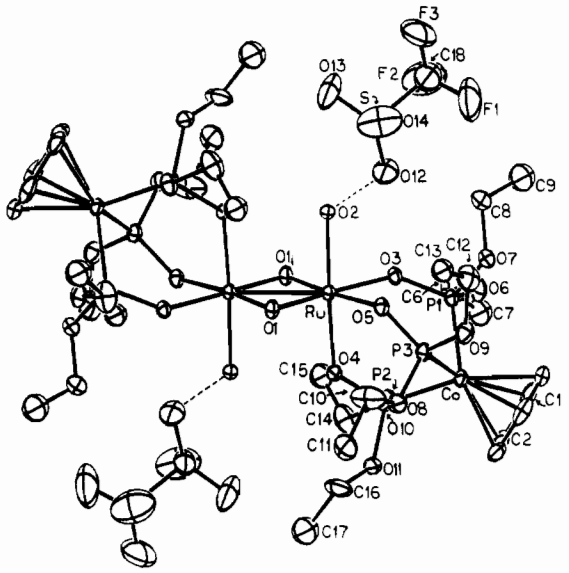

Figure 1. ORTEP view of $[L_{OEt}(H_2O)Ru(\mu\text{-}O)_2Ru(OH_2)L_{OEt}][CF_3SO_3]_2$ showing the close interaction of the triflate anion with the aquo ligands. Thermal ellipsoids are at the 30% probability level.

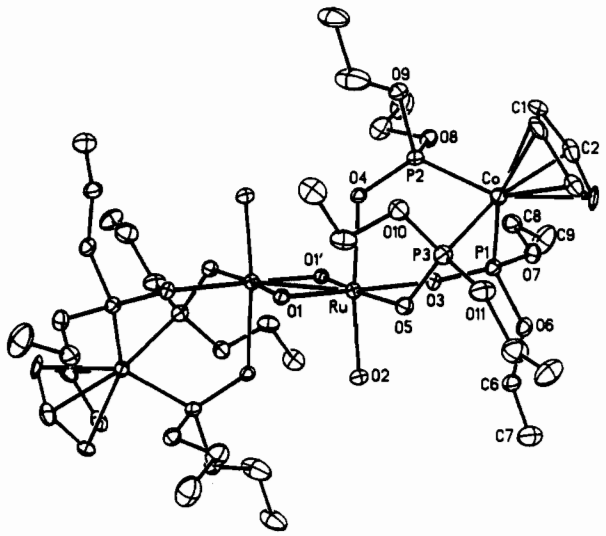

Figure 2. ORTEP view of $[L_{OEt}(HO)Ru(\mu\text{-}O)_2Ru(OH)L_{OEt}]$ with 30% probability ellipsoids.

Results

The syntheses of the novel, dimeric, edge-sharing ruthenium(IV) aquo and hydroxo complexes $[L_{OEt}(H_2O)Ru(\mu\text{-}O)_2Ru(OH_2)L_{OEt}][X]_2$ (X = PF_6, CF_3SO_3) and $[L_{OEt}(HO)Ru(\mu\text{-}O)_2Ru(OH)L_{OEt}]$ are described. A rare ruthenium(V) oxo species, $[L_{OEt}(O)Ru(\mu\text{-}O)_2Ru(O)L_{OEt}]$, was obtained by treatment of the hydroxo complex with $Ru^{VIII}O_4$. The analytical and spectral data for all four complexes are given in the Experimental Section.

$[L_{OEt}(H_2O)Ru(\mu\text{-}O)_2Ru(OH_2)L_{OEt}][CF_3SO_3]_2$, $[L_{OEt}(HO)Ru(\mu\text{-}O)_2Ru(OH)L_{OEt}]$, and $[L_{OEt}(O)Ru(\mu\text{-}O)_2Ru(O)L_{OEt}]$ were structurally characterized by single-crystal X-ray diffraction

(6) (a) *International Tables for X-ray Crystallography*; Kynoch Press: Birmingham, U.K., 1974; Vol. IV, pp 71, 149. (b) Program XABS: H. Hope and B. Moezzi, University of California, Davis. The program obtains an absorption tensor from F_o–F_c differences. Moezzi, B. Ph.D. Dissertation, University of California, Davis, 1987.

Table I. Crystal Data for $[L_{OEt}(H_2O)Ru(\mu\text{-}O)_2Ru(OH_2)L_{OEt}][CF_3SO_3]_2$, $[L_{OEt}(HO)Ru(\mu\text{-}O)_2Ru(OH)L_{OEt}]\cdot 4C_6H_5CH_3$, and $[L_{OEt}(O)Ru(\mu\text{-}O)_2Ru(O)L_{OEt}]$

formula	$Ru_2Co_2C_{36}H_{74}O_{28}P_6S_2F_6$	$Ru_2Co_2C_{62}H_{104}O_{22}P_6$	$Ru_2Co_2C_{34}H_{70}O_{22}P_6$
fw	1635.08	1705.35	1336.92
cyst syst	triclinic	monoclinic	monoclinic
space group	$P\bar{1}$ (No. 2)	$P2_1/n$ (No. 14)	$C2/c$ (No. 15)
a/Å	10.510 (6)	13.187 (5)	27.486 (7)
b/Å	13.475 (6)	23.103 (8)	11.849 (5)
c/Å	14.132 (9)	13.455 (6)	17.268 (7)
α/deg	101.50 (5)		
β/deg	117.99 (5)	113.82 (4)	109.11 (3)
γ/deg	101.42 (5)		
V/Å^3	1630.6 (16)	3750 (3)	5314 (5)
Z	1	2	4
T/K	294	130	294
λ/Å	0.71073	0.71069	0.71073
μ/cm^{-1}	12.67	10.14	14.38
ρ_{calcd}/g cm^{-3}	1.66	1.51	1.72
R	0.0483	0.0563	0.0610
GOF (param; refl)	2.65 (3.70; 5718)	1.26 (378; 3439)	1.85 (303; 4070)

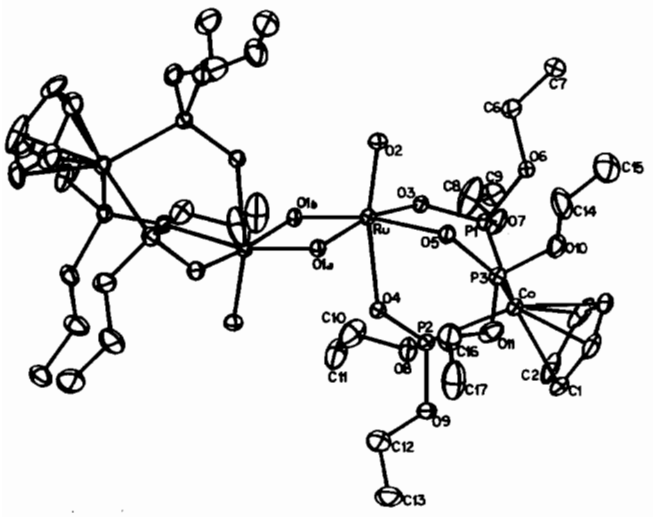

Figure 3. ORTEP view of $[L_{OEt}(O)Ru(\mu\text{-}O)_2Ru(O)L_{OEt}]$ with 30% probability ellipsoids.

studies. Figures 1–3 show the ORTEP plots of $[L_{OEt}(H_2O)Ru(\mu\text{-}O)_2Ru(OH_2)L_{OEt}][CF_3SO_3]_2$, $[L_{OEt}(HO)Ru(\mu\text{-}O)_2Ru(OH)L_{OEt}]$, and $[L_{OEt}(O)Ru(\mu\text{-}O)_2Ru(O)L_{OEt}]$, respectively. Figure 4 shows only the core geometries of the ruthenium atoms and the terminal and bridging oxygen ligands associated with each structure along with the pertinent bond distances and angles. Table V contains other selected bond distances and angles relevant to the core geometries of the three structures.

The syntheses, along with the spectroscopic and structural characteristics of the title complexes are discussed in the following sections.

Discussion

Synthesis and Spectral Data for $[L_{OEt}(H_2O)Ru(\mu\text{-}O)_2Ru(OH_2)L_{OEt}][X]_2$ (X = PF_6, CF_3SO_3) and $[L_{OEt}(HO)Ru(\mu\text{-}O)_2Ru(OH)L_{OEt}]$. The most common approach to synthesizing high-oxidation-state ruthenium oxo complexes involves the oxidation of low-valent (primarily Ru^{II}) derivatives containing a tightly bound ancillary ligand and some relatively labile ligand such as H_2O or CO. This approach has been very successful in the hands of Che, Meyer, and Groves and their co-workers, particularly with respect to the synthesis of *trans*-$Ru^{VI}O_2$ systems.[1] An earlier more direct approach, developed by Griffith and co-workers, involves the use of $Ru^{VIII}O_4$ as both a source of ruthenium and of oxo ligand.[5] We have used a combination of both of these approaches to attach the L_{OEt}^- ligand to ruthenium and to access a terminal-oxo derivative.

Treatment of a 1% H_2SO_4 solution of NaL_{OEt} with a CCl_4 solution of RuO_4 generates a green aqueous layer that contains $[L_{OEt}(H_2O)Ru(\mu\text{-}O)_2Ru(OH_2)L_{OEt}][SO_4]$ (Scheme I). The dication of $[L_{OEt}(H_2O)Ru(\mu\text{-}O)_2Ru(OH_2)L_{OEt}][PF_6]_2$ can be

Scheme I

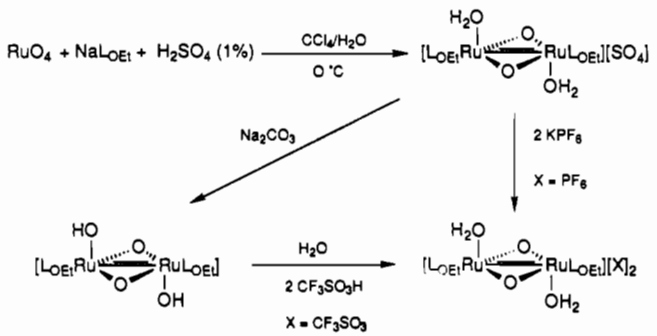

isolated from this solution by metathesis with KPF_6 (however, see below). Alternatively, treatment with excess base (Na_2CO_3 or NaOH) gives the neutral, benzene-soluble product, $[L_{OEt}(HO)Ru(\mu\text{-}O)_2Ru(OH)L_{OEt}]$. In turn, $[L_{OEt}(HO)Ru(\mu\text{-}O)_2Ru(OH)L_{OEt}]$ can be treated with CF_3SO_3H to generate $[L_{OEt}(H_2O)Ru(\mu\text{-}O)_2Ru(OH_2)L_{OEt}][CF_3SO_3]_2$. Indeed, it is preferable to isolate the dication of $[L_{OEt}(H_2O)Ru(\mu\text{-}O)_2Ru(OH_2)L_{OEt}][PF_6]_2$ by reprotonating $[L_{OEt}(HO)Ru(\mu\text{-}O)_2Ru(OH)L_{OEt}]$ with dilute sulfuric acid, followed by metathesis with KPF_6. This procedure, via $[L_{OEt}(HO)Ru(\mu\text{-}O)_2Ru(OH)L_{OEt}]$, leads to very pure samples of the dications. The dications of $[L_{OEt}(H_2O)Ru(\mu\text{-}O)_2Ru(OH_2)L_{OEt}][X]_2$ (X = PF_6, CF_3SO_3), which have been isolated in this manner, and $[L_{OEt}(HO)Ru(\mu\text{-}O)_2Ru(OH)L_{OEt}]$ are stable indefinitely both in solution and in the solid state. The use of 1% acid as opposed to e.g. 5% or 0.5% is critical with respect to the yield. If the reaction is done without acid, no identifiable products can be isolated. Acid is presumably required to neutralize excess oxide equivalents produced in the RuO_4 reduction. An unexpected byproduct of the synthesis, which can be isolated in about 20% yield from the CCl_4 layer, is the L_{OEt}^- analogue of ruthenocene, $(L_{OEt})_2Ru^{II}$.[7]

The NMR data for all three complexes are indicative of diamagnetic species. The ^1H and the $^{31}P\{^1H\}$ NMR spectra clearly suggest an $L_{OEt}RuX_2Y$ type configuration for both systems, although the differences in splitting and shift patterns between the dications and the neutral complex are quite distinctive despite a relatively minor change in the coordination sphere of the ruthenium atom ($H_2O \rightarrow OH$). (The origin of the splitting pattern for the $L_{OEt}RuX_2Y$ configuration with C_s symmetry has previously been discussed.[8]) The assignments of the NMR signals for the aquo protons of $[L_{OEt}(H_2O)Ru(\mu\text{-}O)_2Ru(OH_2)L_{OEt}][PF_6]_2$ and $[L_{OEt}(H_2O)Ru(\mu\text{-}O)_2Ru(OH_2)L_{OEt}][CF_3SO_3]_2$ are based on their

(7) Bercaw, J. E.; Labinger, J. A.; Power, J. M. Unpublished work. This is a new compound and has been characterized by elemental analysis, by ^1H NMR and IR spectroscopy, and by its similarity to the iron derivative, $(L_{OEt})_2Fe$ (see ref 4b).

(8) Kläui, W.; Müller, A. *J. Organomet. Chem.* **1983**, *253*, 45.

Table II. Final Non-Hydrogen Coordinates, Displacement Parameters, and Atom Populations for $[L_{OEt}(H_2O)Ru(\mu\text{-}O)_2Ru(OH_2)L_{OEt}][CF_3SO_3]_2$ (x, y, z, and U_{eq}[a] $\times 10^4$)

atom	x	y	z	U_{eq} or B/Å^2
Ru	1202 (0.4)	792 (0.3)	476 (0.3)	436 (1)
O1	−795 (3)	719 (3)	167 (3)	545 (9)
O2	680 (4)	962 (3)	−1061 (2)	577 (9)
O3	3397 (3)	1034 (2)	850 (3)	505 (8)
O4	1847 (3)	664 (3)	2058 (2)	528 (8)
O5	1858 (3)	2423 (2)	1142 (3)	509 (8)
P1	4859 (1)	1943 (1)	1802 (1)	498 (3)
P2	3467 (1)	1170 (1)	3137 (1)	504 (3)
P3	3006 (1)	3144 (1)	2379 (1)	521 (3)
Co	4936 (0.7)	2667 (0.5)	2244 (0.5)	492 (2)
O6	6215 (4)	1509 (3)	1994 (3)	712 (11)
O7	5211 (4)	2885 (3)	1346 (3)	677 (9)
O8	2145 (4)	3259 (3)	3045 (3)	699 (10)
O9	3495 (5)	4322 (3)	2352 (3)	756 (11)
O10	4313 (4)	309 (3)	3210 (3)	702 (10)
O11	3207 (4)	1213 (3)	4158 (3)	743 (11)
C1	7276 (7)	3024 (7)	4390 (7)	960 (26)
C2	6596 (9)	2803 (6)	4967 (6)	1003 (26)
C3	5872 (8)	3534 (8)	5037 (5)	960 (25)
C4	6123 (9)	4209 (5)	4495 (7)	1005 (26)
C5	6981 (8)	3888 (7)	4082 (5)	978 (25)
C6	6130 (8)	428 (7)	1793 (8)	1183 (26)
C7	7432 (19)	207 (13)	2562 (21)	10.2 (6)[b]
C7′	7504 (21)	279 (14)	2003 (21)	6.6 (7)[b]
C8	4974 (9)	2647 (7)	218 (6)	1096 (24)
C9	6292 (23)	2804 (16)	232 (15)	10.9 (7)[b]
C9′	5724 (24)	3435 (18)	7 (17)	8.6 (8)[b]
C10	789 (10)	3556 (10)	2595 (7)	1520 (31)
C11	132 (8)	3570 (7)	3269 (7)	1119 (24)
C12	3164 (10)	4587 (6)	1334 (7)	1079 (24)
C13	1856 (19)	4946 (12)	868 (13)	7.4 (5)[b]
C13′	3106 (38)	5669 (27)	1590 (26)	14.8 (11)[b]
C14	3657 (10)	−748 (6)	3199 (9)	1176 (26)
C15	3254 (22)	−1542 (12)	2205 (16)	8.7 (5)[b]
C15′	4209 (31)	−1548 (16)	2882 (22)	8.2 (8)[b]
C16	1928 (9)	1322 (9)	4184 (6)	1268 (27)
C17	1449 (31)	626 (36)	4696 (27)	11.0 (9)[b]
C17′	1852 (44)	1224 (50)	5112 (39)	11.2 (12)[b]
S	339 (3)	2962 (2)	7537 (2)	1271 (8)
O12	1124 (7)	2828 (4)	8614 (4)	1347 (19)
O13	−600 (8)	1974 (5)	6577 (6)	1863 (30)
O14	−208 (11)	3892 (7)	7499 (7)	2183 (32)
C18	1800 (20)	3470 (13)	7247 (12)	2033 (63)
F1	2737 (9)	4339 (7)	8040 (9)	2701 (43)
F2	2374 (13)	2638 (10)	7318 (8)	2779 (46)
F3	1165 (10)	3598 (8)	6288 (7)	2704 (38)

atom	population	atom	population
C(7)	0.62 (4)	C(15)	0.60 (3)
C(9)	0.59 (3)	C(17)	0.59 (7)
C(13)	0.52 (2)		

[a] $U_{eq} = {}^1/_3\sum_i\sum_j[U_{ij}(a_i^*a_j^*)(\vec{a}_i\vec{a}_j)]$. [b] Isotropic displacement parameter, B.

disappearance upon addition of D_2O and on their appropriate integral values.

The IR spectra for the three complexes $[L_{OEt}(H_2O)Ru(\mu\text{-}O)_2Ru(OH_2)L_{OEt}][X]_2$ (X = PF_6, CF_3SO_3) and $[L_{OEt}(HO)Ru(\mu\text{-}O)_2Ru(OH)L_{OEt}]$ are dominated by bands due to the L_{OEt}^- ligand. The bands above 3000 cm^{-1} indicate the presence of O–H bonds; interestingly, in the case of $[L_{OEt}(H_2O)Ru(\mu\text{-}O)_2Ru(OH_2)L_{OEt}][CF_3SO_3]_2$ this band appears at a relatively low frequency (3126 cm^{-1}). The UV–vis spectra exhibit intense absorption maxima at ca. 240 and 340 nm, which are presumably CT bands associated with the L_{OEt}^- ligand, since the UV–vis spectrum of $L_{OEt}Na$ also exhibits intense maxima at these wavelengths. The relatively weak absorptions in the visible region are possibly due to d–d transitions and are responsible for the green color of these complexes.

Synthesis and Spectral Data for $[L_{OEt}(O)Ru(\mu\text{-}O)_2Ru(O)L_{OEt}]$. The most common oxidants used to generate ruthenium oxo species from low-valent derivatives have been oxo atom transfer reagents such as H_2O_2, Me_3COOH, *m*-chloroperbenzoic acid, and C_6H_5IO. In some cases outer-sphere oxidants such as Ce^{IV} have also been used. While RuO_4 is generally found to be a very unselective oxidant, particularly toward organic substrates,[9] we have discovered that it reacts with the neutral hydroxy complex $[L_{OEt}(HO)Ru(\mu\text{-}O)_2Ru(OH)L_{OEt}]$ to give the neutral ruthenium(V) complex $[L_{OEt}(O)Ru(\mu\text{-}O)_2Ru(O)L_{OEt}]$ in good yield (eq 1).

$$[L_{OEt}(HO)Ru(\mu\text{-}O)_2Ru(OH)L_{OEt}] + RuO_4 \xrightarrow{CCl_4} [L_{OEt}(O)Ru(\mu\text{-}O)_2Ru(O)L_{OEt}] + \text{“}(HO)_2RuO_2\text{”} \quad (1)$$

Black, polymeric $Ru^{IV}O_2$, a common byproduct of RuO_4 oxidations, is not produced in the reaction. From the stoichiometry, a simple byproduct would be the unknown ruthenic acid, $(HO)_2Ru^{IV}O_2$. Washing the reaction mixture with aqueous KOH produces a material that shows UV–vis and IR bands characteristic of ruthenate, RuO_4^{2-}, which is consistent with the above byproduct.

Table III. Final Non-Hydrogen Coordinates ($\times 10^4$) and Displacement Parameters (Å$^2 \times 10^3$) for $[L_{OEt}(HO)Ru(\mu\text{-}O)_2Ru(OH)L_{OEt}]$

	x	y	z	U
Ru	9243 (1)	148 (1)	4148 (1)	19 (1)[a]
O1	10310 (4)	603 (2)	5244 (4)	20 (2)[a]
O2	10112 (4)	113 (2)	3261 (4)	24 (2)[a]
O3	7952 (4)	−270 (2)	2890 (4)	20 (2)[a]
O4	8125 (4)	231 (2)	4934 (4)	22 (2)[a]
O5	8557 (4)	909 (2)	3302 (4)	24 (2)[a]
P1	6873 (2)	−3 (1)	2115 (2)	22 (1)[a]
P2	6865 (2)	206 (1)	4373 (2)	23 (1)[a]
P3	7462 (2)	1183 (1)	3206 (2)	26 (1)[a]
Co	6053 (1)	601 (1)	2785 (1)	22 (1)[a]
O6	7036 (4)	301 (2)	1127 (4)	25 (2)[a]
O7	6103 (4)	−538 (2)	1487 (4)	29 (2)[a]
O8	6452 (4)	−442 (2)	4284 (4)	26 (2)[a]
O9	6419 (4)	460 (3)	5236 (4)	32 (2)[a]
O10	7614 (4)	1530 (2)	4280 (4)	30 (2)[a]
O11	7249 (5)	1727 (3)	2414 (5)	38 (3)[a]
C1	4546 (7)	566 (4)	2941 (7)	34 (4)[a]
C2	4469 (7)	271 (4)	1996 (7)	34 (4)[a]
C3	4669 (7)	671 (4)	1309 (7)	28 (4)[a]
C4	4897 (7)	1203 (5)	1848 (8)	41 (4)[a]
C5	4827 (7)	1142 (4)	2856 (8)	36 (4)[a]
C6	7842 (7)	48 (4)	748 (7)	31 (4)[a]
C7	8116 (9)	495 (5)	89 (8)	51 (5)[a]
C8	6073 (7)	−1072 (4)	2014 (7)	37 (4)[a]
C9	5721 (11)	−1534 (5)	1208 (8)	64 (6)[a]
C10	7088 (8)	−851 (4)	5148 (7)	42 (4)[a]
C11	6476 (10)	−1400 (4)	4997 (9)	59 (5)[a]
C12	6954 (10)	864 (6)	6038 (10)	90 (7)[a]
C13	6597 (9)	958 (6)	6844 (9)	72 (6)[a]
C14	8655 (7)	1828 (4)	4859 (7)	39 (4)[a]
C15	8549 (8)	2217 (4)	5693 (8)	40 (4)[a]
C16	7387 (8)	1715 (4)	1430 (8)	47 (5)[a]
C17	7117 (9)	2313 (4)	928 (8)	48 (5)[a]
C18	1308 (7)	1309 (4)	2015 (7)	33 (2)
C19	661 (7)	1412 (4)	2587 (7)	29 (2)
C20	585 (8)	1969 (4)	2956 (7)	42 (3)
C21	1189 (8)	2424 (5)	2783 (8)	49 (3)
C22	1882 (8)	2310 (4)	2252 (8)	46 (3)
C23	1907 (7)	1758 (4)	1870 (7)	38 (2)
C24	1356 (8)	714 (4)	1581 (8)	52 (3)
C25	9847 (8)	1866 (4)	8980 (8)	45 (3)
C26	10590 (8)	2238 (4)	8847 (8)	46 (3)
C27	11153 (9)	2081 (5)	8203 (8)	59 (3)
C28	10948 (9)	1555 (5)	7726 (9)	61 (3)
C29	10236 (8)	1184 (5)	7841 (8)	54 (3)
C30	9683 (8)	1327 (4)	8480 (8)	48 (3)
C31	9254 (11)	2019 (6)	9686 (11)	86 (4)

[a] Equivalent isotropic U defined as one-third of the trace of the orthogonalized U_{ij} tensor.

(9) Seddon, E. A.; Seddon, K. R. In *The Chemistry of Ruthenium*; Elsevier: Amsterdam, 1984; p 43. Schröder, M.; Stephenson, T. A. In *Comprehensive Coordination Chemistry*; Wilkinson, G., Gillard, R. D., McCleverty, J. A., Eds.; Pergamon Press: New York, 1987; p 423 and references cited therein.

Table IV. Final Non-Hydrogen Coordinates and Displacement Parameters for $[L_{OEt}(O)Ru(\mu\text{-}O)_2Ru(O)L_{OEt}]$ (x, y, z, and $U_{eq}{}^a \times 10^4$)

atom	x	y	z	U_{eq}
Ru	204 (0.1)	2212 (0.3)	1821 (0.2)	535 (1)
O1a	0	3217 (3)	2500	579 (9)
O1b	0	1199 (3)	2500	578 (9)
O2	−304 (1)	2160 (2)	913 (2)	716 (8)
O3	604 (1)	991 (2)	1344 (2)	583 (6)
O4	946 (1)	2316 (2)	2763 (2)	651 (7)
O5	525 (1)	3497 (2)	1277 (2)	651 (7)
P1	1038	1205 (1)	1005 (1)	613 (3)
P2	1481	2119 (1)	2743 (1)	622 (3)
P3	1067	3756 (1)	1312 (1)	671 (3)
Co	1631 (0.2)	2420 (0.5)	1611 (0.3)	632 (1)
O6	809 (1)	1516 (3)	57 (2)	834 (9)
O7	1311 (1)	35 (3)	984 (2)	954 (10)
O8	1661 (1)	880 (3)	3066 (2)	893 (9)
O9	1866 (1)	2888 (3)	2440 (2)	951 (10)
O10	1055 (1)	4281 (3)	462 (2)	1025 (11)
O11	1274 (1)	4801 (3)	1908 (3)	1054 (11)
C1	2363 (2)	3063 (9)	2086 (5)	1131 (23)
C2	2384 (2)	1898 (11)	2041 (7)	1439)30)
C3	2171 (3)	1625 (8)	1205 (10)	1545 (32)
C4	2043 (2)	2639 (11)	826 (4)	1298 (24)
C5	2155 (2)	3468 (6)	1349 (7)	1163 (22)
C6	332 (2)	1179 (7)	−464 (3)	1323 (23)
C7	196 (2)	1487 (5)	−1293 (3)	1062 (18)
C8	1160 (3)	−978 (6)	1006 (7)	1802 (32)
C9	1425 (2)	−1908 (5)	861 (4)	1072 (17)
C10	1371 (3)	169 (6)	3388 (5)	1421 (24)
C11	1597 (2)	−712 (6)	3812 (5)	1441 (24)
C12	1795 (3)	3174 (7)	4145 (4)	1367 (23)
C13	2120 (3)	4062 (6)	4612 (4)	1336 (22)
C14	668 (3)	4808 (9)	−85 (5)	1850 (35)
C15	609 (3)	4946 (7)	−852 (5)	1532 (27)
C16	977 (4)	5444 (8)	2255 (5)	1798 (31)
C17	1156 (4)	6401 (7)	2625 (6)	1894 (34)

$^a U_{eq} = {}^1/_3\sum_i\sum_j[U_{ij}(a_i{}^*a_j{}^*)(\vec{a}_i\cdot\vec{a}_j)]$.

Analytically pure $[L_{OEt}(O)Ru(\mu\text{-}O)_2Ru(O)L_{OEt}]$ can be obtained by washing of the filtered reaction mixture with dilute $NaHCO_3$, followed by recrystallization from CCl_4/*n*-pentane at −60 °C. The oxo complex is stable in the solid state but is best stored under a dry, anaerobic atmosphere. It oxidizes primary and secondary alcohols to the corresponding aldehydes and ketones and gives the parent bis(hydroxo) Ru^{IV}–Ru^{IV} complex, $[L_{OEt}(HO)Ru(\mu\text{-}O)_2Ru(OH)L_{OEt}]$, as the reduced ruthenium species (e.g. eq 2).

$$[L_{OEt}(O)Ru(\mu\text{-}O)_2Ru(O)L_{OEt}] + i\text{-}C_3H_7OH \xrightarrow{CCl_4,\ 3\ h,\ 25\ °C} [L_{OEt}(HO)Ru(\mu\text{-}O)_2Ru(OH)L_{OEt}] + (CH_3)_2C{=}O \quad (2)$$

The ^1H NMR spectrum of $[L_{OEt}(O)Ru(\mu\text{-}O)_2Ru(O)L_{OEt}]$ clearly shows the d^3–d^3 system to be diamagnetic, implying some coupling mechanism for the unpaired spins (see next section). The spectrum displays the expected pattern for the $L_{OEt}{}^-$ ligand in C_s symmetry, although again the splitting pattern is quite distinct from that of the parent $[L_{OEt}(HO)Ru(\mu\text{-}O)_2Ru(OH)L_{OEt}]$. The IR spectrum is remarkably similar to that of the hydroxy complex except for the appearance of a single new band at 848 cm^{-1}, which we very tentatively assign to the $\nu(Ru{=}O)$ stretch. This value is slightly lower than the range found for the few known $Ru^V{=}O$ complexes (908–860 cm^{-1}), although it corresponds well with the Ru=O distance found in the X-ray structure (next section). It is also possible that bands associated with the $L_{OEt}{}^-$ ligand may be obscuring a higher value for this mode around 900 cm^{-1}. The UV–vis spectrum shows a shift (ca. 100 nm) to higher energy of the low-intensity band found in the visible region of the spectra of the Ru^{IV}–Ru^{IV} complexes. This blue shift is manifested in a corresponding color change from green to purple.

Structures and Metal–Metal Bonding of $[L_{OEt}(H_2O)Ru(\mu\text{-}O)_2Ru(OH_2)L_{OEt}][CF_3SO_3]_2$, $[L_{OEt}(HO)Ru(\mu\text{-}O)_2Ru(OH)L_{OEt}]$, and $[L_{OEt}(O)Ru(\mu\text{-}O)_2Ru(O)L_{OEt}]$. In $[L_{OEt}(H_2O)Ru(\mu\text{-}O)_2Ru(OH_2)L_{OEt}][CF_3SO_3]_2$ and $[L_{OEt}(HO)Ru(\mu\text{-}O)_2Ru(OH)L_{OEt}]$, a center of symmetry between the two ruthenium atoms relates the halves of the dimers. In $[L_{OEt}(O)Ru(\mu\text{-}O)_2Ru(O)L_{OEt}]$ the halves of the dimer are related by a crystallographically imposed C_2 axis that passes through the bridging oxygen atoms. All three structures belong to the general class of edge-sharing bioctahedral complexes, where the ideal D_{2h} symmetry is lowered to C_{2h}, the shared edge being occupied by the two bridging oxo ligands. Each molecule of $[L_{OEt}(HO)Ru(\mu\text{-}O)_2Ru(OH)L_{OEt}]$ has four toluene molecules of solvation associated with it, which accounts for the loss of crystallinity when single crystals of this complex are isolated. The parameters associated with the $L_{OEt}{}^-$ ligands are unre-

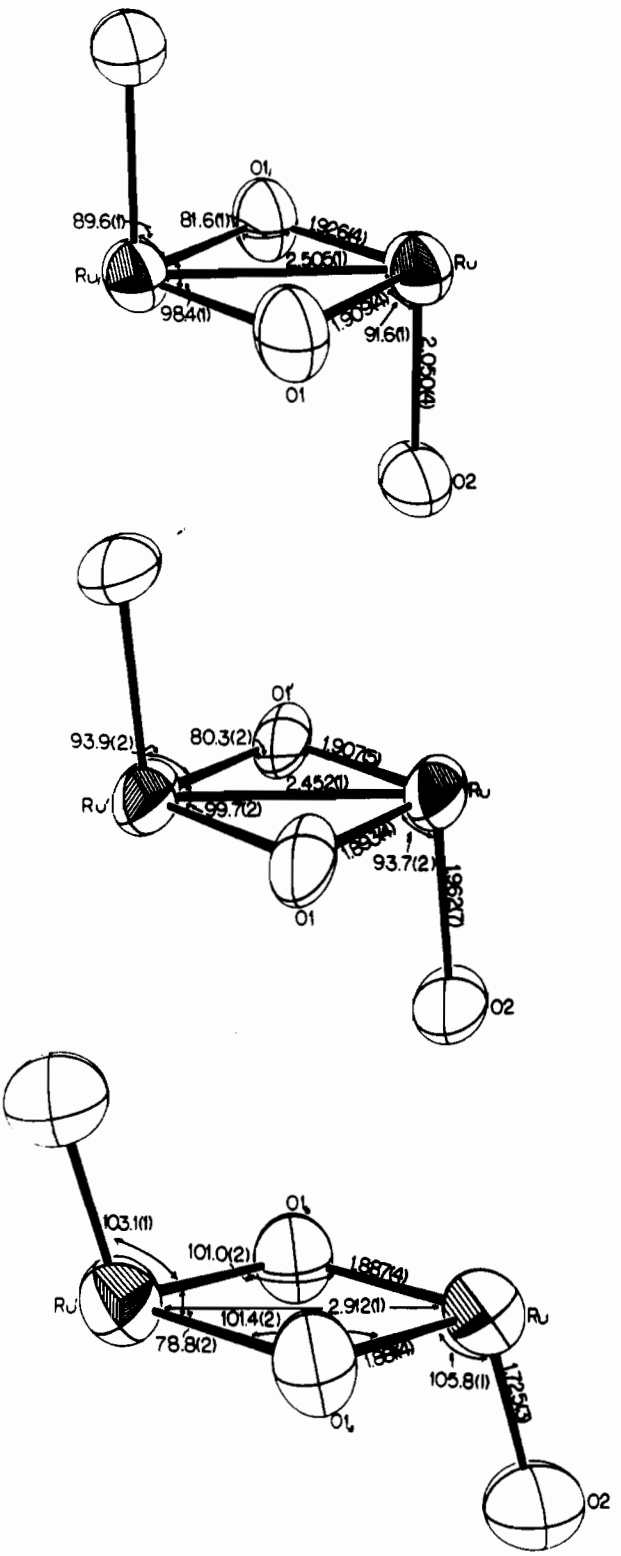

Figure 4. Ruthenium atom and terminal and bridging oxygen ligand cores of $[L_{OEt}(H_2O)Ru(\mu\text{-}O)_2Ru(OH_2)L_{OEt}][CF_3SO_3]_2$, $[L_{OEt}(HO)Ru(\mu\text{-}O)_2Ru(OH)L_{OEt}]$, and $[L_{OEt}(O)Ru(\mu\text{-}O)_2Ru(O)L_{OEt}]$ with pertinent bond distances (Å) and angles (deg).

Table V. Selected Core Distances (Å) and Angles (deg) Not Given in Figure 4

	$[L_{OEt}(H_2O)Ru(\mu\text{-}O)_2Ru(OH_2)L_{OEt}]$	$[L_{OEt}(HO)Ru(\mu\text{-}O)_2Ru(OH)L_{OEt}]$	$[L_{OEt}(O)Ru\mu\text{-}O)_2Ru(O)L_{OEt}]$
Ru–O3	2.048 (3)	2.091 (4)	2.138 (3)
Ru–O4	2.065 (3)	2.142 (6)	2.157 (3)
Ru–O5	2.039 (3)	2.090 (5)	2.127 (3)
O3–Ru–O1	174.3 (1)	173.5 (2)	164.6 (1)
O3–Ru–O1$_i$[a]	87.2 (1)	86.3 (2)	95.9 (1)
O3–Ru–O2	87.3 (1)	88.4 (2)	89.5 (1)
O4–Ru–O1	91.1 (1)	90.5 (2)	83.9 (1)
O4–Ru–O1$_i$	91.4 (1)	91.4 (2)	88.2 (1)
O4–Ru–O2	177.0 (1)	172.6 (2)	166.3 (1)
O4–Ru–O3	89.9 (1)	86.8 (2)	81.4 (1)
O4–Ru–O5	90.7 (1)	87.8 (2)	82.2 (1)
O5–Ru–O1	898.1 (1)	88.8 (2)	94.2 (1)
O5–Ru–O1	173.1 (1)	171.5 (2)	168.7 (1)
O5–Ru–O2	88.0 (1)	86.2 (2)	87.3 (1)
O5–Ru–O3	86.2 (1)	85.2 (2)	88.5 (1)
P1–O3–Ru	128.5 (2)	126.9 (3)	127.3 (2)
P2–O4–Ru	126.3 (2)	125.6 (3)	131.7 (2)
P3–O5–Ru	127.7 (2)	125.4 (4)	132.7 (2)

[a] O1′ in $[L_{OEt}(HO)Ru(\mu\text{-}O)_2Ru(OH)L_{OEt}]$ and O1b in $[L_{OEt}(O)Ru(\mu\text{-}O)_2Ru(O)L_{OEt}]$.

markable.[4e,f,10] The most important parameters are those associated with the terminal and bridging oxygen ligands and the Ru–Ru separation.

The Ru–O2 distance in $[L_{OEt}(H_2O)Ru(\mu\text{-}O)_2Ru(OH_2)L_{OEt}][CF_3SO_3]_2$, 2.050 (4) Å, is within the range found for Ru–OH_2 bonds[3b,11] and is markedly longer than that found for the Ru–OH bond in $[L_{OEt}(HO)Ru(\mu\text{-}O)_2Ru(OH)L_{OEt}]$, 1.962 (7) Å. (Interestingly, in $[L_{OEt}(H_2O)Ru(\mu\text{-}O)_2Ru(OH_2)L_{OEt}][CF_3SO_3]_2$ the aquo ligands are found to be hydrogen-bonded to the triflate anions ($O2_{aq}\cdots O12_{OTf}$ = 2.636 (7) Å; see Figure 1).) As expected, there is a dramatic shortening of the Ru–O2 distance in $[L_{OEt}(O)Ru(\mu\text{-}O)_2Ru(O)L_{OEt}]$ to a value of 1.725 (3) Å, indicative of an Ru=O bond. Ruthenium(V) complexes are relatively rare, and there are only two other structural reports of Ru^V=O complexes. The Ru=O bond is somewhat longer than the very short value of 1.686 (6) Å found in $[RuO(O_2COCEt_2)_2][(CH_3CH_2CH_2)_4N]$ (ν(Ru=O) = 900 cm^{-1})[12a] but is slightly shorter than the value of 1.733 (6) Å found in $[RuO(CH_2SiMe_3)_3]_2$ (ν(Ru=O) = 908 cm^{-1}).[12b] The oxo ligands in the latter complex are semibridging, and therefore a comparison may not be justified. It is also noteworthy that in these two examples the ruthenium atoms display trigonal-bipyramidal geometry with the oxo ligands in equatorial positions, whereas the octahedral geometry of the ruthenium centers in $[L_{OEt}(O)Ru(\mu\text{-}O)_2Ru(O)L_{OEt}]$ dictate that the oxo ligand has another ligand trans to itself, which may account for the longer R=O distance. This may also account for the lower ν(Ru=O) value of 848 cm^{-1} in the IR spectrum of $[L_{OEt}(O)Ru(\mu\text{-}O)_2Ru(O)L_{OEt}]$ (see previous section). Furthermore, Che and co-workers recently described the synthesis of a mononuclear ruthenium(V) oxo complex with octahedral geometry. Although the complex was not structurally characterized, an intense band at 872 cm^{-1} was assigned to the ν(Ru=O) stretch, a value that is intermediate between those for the above two systems and the present case.[13]

The Ru–O1 distances are consistent with bridging oxo ligands. They do not vary a great deal, although the average value in $[L_{OEt}(O)Ru(\mu\text{-}O)_2Ru(O)L_{OEt}]$ is, as might be expected ($Ru^{IV} \rightarrow Ru^V$), somewhat shorter than in $[L_{OEt}(H_2O)Ru(\mu\text{-}O)_2Ru(OH_2)L_{OEt}][CF_3SO_3]_2$ and $[L_{OEt}(HO)Ru(\mu\text{-}O)_2Ru(OH)L_{OEt}]$.

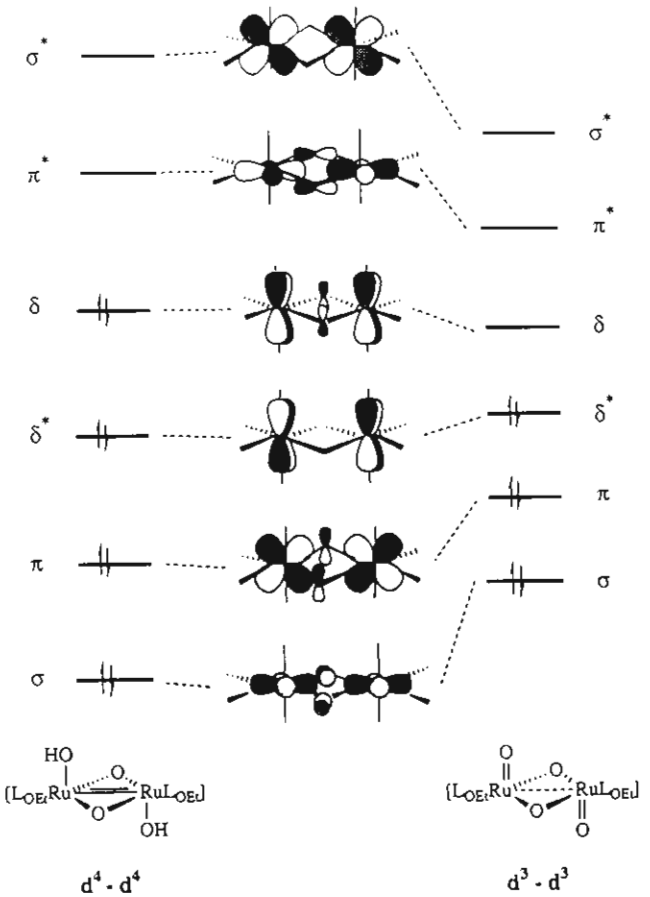

Figure 5. Qualitative molecular orbital representation of the metal–metal interaction in the edge-sharing Ru^{IV}–Ru^{IV} and Ru^V–Ru^V complexes (see ref 14).

Perhaps the most interesting parameter in all three structures is the Ru–Ru separation. In the Ru^{IV} complexes $[L_{OEt}(H_2O)Ru(\mu\text{-}O)_2Ru(OH_2)L_{OEt}][CF_3SO_3]_2$ and $[L_{OEt}(HO)Ru(\mu\text{-}O)_2Ru(OH)L_{OEt}]$ this value is clearly indicative of a fairly strong metal–metal interaction. The slightly longer value in the former is presumably due to increased Coulombic repulsion between the two ruthenium centers. In the Ru^V compound $[L_{OEt}(O)Ru(\mu\text{-}O)_2Ru(O)L_{OEt}]$ however, this value increases considerably (almost 0.5 Å longer than that in $[L_{OEt}(HO)Ru(\mu\text{-}O)_2Ru(OH)L_{OEt}]$) and is suggestive of little or no metal-metal interaction. These ob-

(10) Kläui, W.; Lenders, B.; Hessner, B.; Evertz, K. *Organometallics* **1988**, *7*, 1357.
(11) Dong, V.; Keller, H. J.; Endres, H.; Moroni, W.; Nothe, D. *Acta Crystallogr., Sect. B* **1977**, *B33*, 2428. Durham, B.; Wilson, S. R.; Hodgson, D. J.; Meyer, T. J. *J. Am. Chem. Soc.* **1980**, *102*, 600. Gilbert, J. A.; Eggleston, D. S.; Murphy, W. R., Jr.; Geselowitz, D. A.; Gersten, S. W.; Hodgson, D. J.; Meyer, T. J. *J. Am. Chem. Soc.* **1985**, *107*, 3855.
(12) (a) Dengel, A. C.; Griffith, W. P.; O'Mahoney, C. A.; Williams, D. J. *J. Chem. Soc., Chem. Commun.* **1989**, 1720. (b) Tooze, R. P.; Wilkinson, G.; Motevalli, M.; Hursthouse, M. B. *J. Chem. Soc., Dalton Trans.* **1986**, 2711.
(13) Che, C.-M.; Yam, V. W.-W.; Mak, T. C. W. *J. Am. Chem. Soc.* **1990**, *112*, 2284.

servations can be rationalized, to some degree, by examining the molecular orbitals available for metal–metal bonding in these bioctahedral systems.[14] There are six d orbitals available for M–M bonding originaing from the two t_{2g} sets of each ruthenium atom. From symmetry considerations they are able to form σ, σ^*, π, π^*, δ, and δ^* combinations whose relative energies are given in Figure 5. The reversal in the ordering of the δ and δ^* levels has its origin in a δ-orbital symmetry match with the bridging oxygen ligands.[14a] The electronic configuration for $[L_{OEt}(H_2O)Ru(\mu\text{-}O)_2Ru(OH_2)L_{OEt}][CF_3SO_3]_2$ and $[L_{OEt}(HO)Ru(\mu\text{-}O)_2Ru(OH)L_{OEt}]$ is d^4–d^4 and therefore implies a double bond ($\sigma^2\pi^2\delta^{*2}\delta^2$), which is consistent with the measured Ru–Ru distances. The d^3–d^3 configuration of $[L_{OEt}(O)Ru(\mu\text{-}O)_2Ru(O)L_{OEt}]$, because of the δ/δ^* reversal, would be expected to exhibit a slightly weaker metal–metal interaction. (Obviously, this reversal is not manifest in the d^4–d^4 case.) However, because the δ orbital is only weakly bonding and the δ^* orbital only weakly antibonding, the reversal alone is not expected to account for the very large increase observed in the Ru–Ru distance. A second and possibly a more compelling factor is the increase in effective nuclear charge ($Ru^{IV} \rightarrow Ru^{V}$), which would lead to less diffuse metal orbitals and hence to a weaker metal–metal interaction (represented as a contraction of the energy levels in Figure 5). This latter factor is presumably the major contributor to the lengthening of the Ru–Ru distance.

Finally, in light of long Ru–Ru separation and presumably weak interaction, it is significant that $[L_{OEt}(O)Ru(\mu\text{-}O)_2Ru(O)L_{OEt}]$ appears to be diamagnetic at room temperature, which must imply some strong coupling of the d^3–d^3 system. Whether this coupling occurs via the weak metal–metal interaction or by some other mechanism, such as superexchange mediated by the bridging oxo ligands, is unknown.[15]

(14) (a) Shaik, S.; Hoffmann, R.; Fisel, C. R.; Summerville, R. H. *J. Am. Chem. Soc.* **1980**, *102*, 4555. (b) Cotton, F. A. *Polyhedron* **1987**, *6*, 667.

Conclusions

The edge-sharing bioctahedral ruthenium complexes $[L_{OEt}(H_2O)Ru(\mu\text{-}O)_2Ru(OH_2)L_{OEt}][CF_3SO_3]_2$, $[L_{OEt}(HO)Ru(\mu\text{-}O)_2Ru(OH)L_{OEt}]$, and $[L_{OEt}(O)Ru(\mu\text{-}O)_2Ru(O)L_{OEt}$ have been synthesized under relatively strong oxidizing conditions. These results, particularly the synthesis of the Ru^V–Ru^V oxo system, clearly indicate the oxidative robustness and the viability of the L_{OEt}^- ligand in high-oxidation-state ruthenium oxo chemistry. The structural studies have revealed a considerable metal-metal interaction in the Ru^{IV}–Ru^{IV} systems, while the Ru^V–Ru^V complex is unexpectedly found to be diamagnetic despite a scant metal–metal interaction. The reactivity of these complexes, particularly the Ru^V–Ru^V oxo complex, will be the topic of future reports.

Acknowledgment. This work was supported by the Caltech Consortium in Chemistry and Chemical Engineering (founding members E. I. du Pont de Nemours and Co., Inc., Eastman Kodak Co., Minnesota Mining and Manufacturing Co., and Shell Development Co.). K.E. thanks the Deutsche Forschungsgemeinschaft (Germany) for a stipend. We thank Professor Philip P. Power and Mr. Steven C. Shoner for the crystal structure of $[L_{OEt}(HO)Ru(\mu\text{-}O)_2Ru(OH)L_{OEt}]$.

Supplementary Material Available: Crystal and intensity collection data (Tables S1–S3); complete distances and angles (Tables S4–S6), and anisotropic thermal displacement parameters (Tables S7–S9) for $[L_{OEt}(H_2O)Ru(\mu\text{-}O)_2Ru(OH_2)L_{OEt}][CF_3SO_3]_2$, $[L_{OEt}(HO)Ru(\mu\text{-}O)_2Ru(OH)L_{OEt}]$, and $[L_{OEt}(O)Ru(\mu\text{-}O)_2Ru(O)L_{OEt}]$ and assigned hydrogen parameters (Tables S10 and S11) for $[L_{OEt}(H_2O)Ru(\mu\text{-}O)_2Ru(OH_2)L_{OEt}][CF_3SO_3]_2$ and $[L_{OEt}(O)Ru(\mu\text{-}O)_2Ru(O)L_{OEt}]$ only (18 pages); observed and calculated structure factors (Tables S12–S14) for all three complexes (67 pages). Ordering information is given on any current masthead page.

(15) Weaver, T. T.; Meyer, T. J.; Adeyemi, S. A.; Brown, G. M.; Eckbert, R. P.; Hatfield, W. E.; Johnson, E. C.; Murray, R. W.; Untereker, D. *J. Am. Chem. Soc.* **1975**, *97*, 3039. Armstrong, J. W.; Robinson, W. R.; Walton, R. A. *Inorg. Chem.* **1983**, *22*, 1301. Neubold, P.; Wieghardt, K.; Nuber, B.; Weiss, J. *Inorg. Chem.* **1989**, *28*, 459.

Contribution from the Departments of Chemistry, Washington University, St. Louis, Missouri 63130, and Louisiana State University, Baton Rouge, Louisiana 70803-1804

Conformational Studies on Nickel, Palladium, and Platinum Homobimetallic Complexes Based on a Binucleating Hexaphosphine Ligand System

Suzanne E. Saum,[1a] Scott A. Laneman,[1b] and George G. Stanley*[,1b]

Received January 24, 1990

The reaction of 2 equiv of $NiCl_2 \cdot 6H_2O$, Na_2PdCl_4, or K_2PtCl_4 with the hexaphosphine ligand system $(Et_2PCH_2CH_2)_2PCH_2P(CH_2CH_2PEt_2)_2$, eHTP, produces the diamagnetic homobimetallic species, $M_2Cl_2(eHTP)^{2+}$ (M = Ni, **2**; Pd, **3**; Pt, **4**) in good yields. Single-crystal X-ray structures were performed on the PF_6^- salts of all three systems: Ni, monoclinic $C2/c$, a = 21.901 (7) Å, b = 18.639 (6) Å, c = 21.964 (6) Å, β = 95.42 (4)°, V = 8926 (7) Å^3, Z = 8; Pd, orthorhombic $P2_12_12_1$, a = 14.646 (1) Å, b = 16.761 (4) Å, c = 17.882 (2) Å, V = 4390 (2) Å^3, Z = 4; Pt, orthorhombic $P2_12_12_1$, a = 13.418 (3) Å, b = 17.795 (6) Å, c = 18.906 (4) Å, V = 4514 (4) Å^3, Z = 4. The final discrepancy indices (R values) are 0.092, 0.039, and 0.035 with quality of fit indicators of 3.25, 1.20, and 1.00 for the Ni, Pd, and Pt structures, respectively. The structure on the nickel bimetallic system reveals a distorted square-planar environment about the nickel atoms with the eHTP ligand adopting a symmetrical bis chelating/bridging open-mode coordination geometry with a Ni–Ni separation of 5.885 (1) Å. The Pd and Pt structures are isomorphous and similar to the Ni complex in the sense that the metal centers have distorted square-planar coordination geometries with one chloride and three phosphine ligands but differ quite substantially from the nickel system in that they have eHTP conformations with partially closed-mode structures and M–M separations of 4.4217 (8) and 4.6707 (9) Å, respectively. van der Waals energy calculations were performed on model systems using the SYBYL molecular mechanics/graphics program. The results demonstrate that there are a variety of accessible low-energy rotational conformations for these M_2(eHTP) bimetallic systems.

Introduction

The hextertiary phosphine $(Et_2PCH_2CH_2)_2PCH_2P(CH_2CH_2PEt_2)_2$, eHTP, possesses an unusual combination of bridging and chelating ligand functionalities: a central bis(phosphino)methane unit fused together with two tridentate, bis chelating moieties. eHTP was designed to act as a powerful binucleating ligand for transition-metal centers, and so far in every reaction in which 2 equiv of a simple mononuclear metal halide has been added to 1 equiv of eHTP a bimetallic complex has been observed.[2,3] An interesting aspect of the coordination chemistry

(1) (a) Washington University. (b) LSU.

(2) Askham, F. R.; Stanley, G. G.; Marques, E. C. *J. Am. Chem. Soc.* **1985**, *107*, 7423.

(3) Saum, S. E.; Askham, F. R.; Fronczek, F. R.; Stanley, G. G. *Organometallics* **1988**, *7*, 1409.

0020-1669/90/1329-5065$02.50/0